

Rings and shells of “dark matter” as MOND artifacts

Mordehai Milgrom¹ and Robert H. Sanders²

ABSTRACT

MOND predicts that a mass, M , contained within its transition radius $r_t \equiv (MG/a_0)^{1/2}$, may exhibit a feature at about that radius in the form of a shell, or projected ring, in the deduced distribution of its phantom dark matter. This occurs despite the absence of any underlying feature in the true (“baryon”) source distribution itself. The phenomenon is similar to the appearance of an event horizon and other unusual physics “in the middle of nothing” near the transition radius of General Relativity MG/c^2 . We consider the possibility that this pure MOND phenomenon is in the basis of the recent finding of such a ring in the galaxy cluster Cl 0024+17 by Jee et al. We find that the parameters of the observed ring can be naturally explained in this way; this feature may therefore turn out to be a direct evidence for MOND. We study this phenomenon in simple, axisymmetric configurations aligned with the line of sight: spherical masses, a dumbbell of spherical masses, and an elongated, thin structure. The properties of the apparent ring: its radius, surface density, and contrast, depend on the form of the MOND interpolating function and on the exact three dimensional distribution of the sources (the thin-lens approximation is quite invalid in MOND). We also comment on the possible appearance of orphan features, marking the Newtonian-to-MOND transition, in high surface brightness galaxies. In particular, we find that previously unexplained structure in the rotation curves of some galaxies may be evidence for such features.

Subject headings: dark matter galaxy clusters: kinematics and dynamics

1. Introduction

Prompted by the recent claim of a ring-like feature in the surface density distribution of the galaxy cluster Cl 0024+17, as deduced from weak-lensing analysis by Jee et al. (2007),

¹Center for Astrophysics, Weizmann Institute of Science Rehovot 76100, Israel

²Kapteyn Astronomical Institute, 9700 AV Groningen, Netherlands

we investigate the occurrence of such features in the modified Newtonian dynamics (MOND; Milgrom 1983a; for reviews see Sanders and McGaugh 2002, Bekenstein 2006, Milgrom 2008). In MOND, unlike Newtonian dynamics, a mass M defines a natural scale length $r_t \equiv (MG/a_0)^{1/2}$ that is unrelated to a scale-length in the mass distribution itself (a_0 is the acceleration constant introduced by MOND). This is the so called transition radius (Milgrom 1983a,b, 1986a). For a concentrated mass it marks the transition from the Newtonian regime at small radii to the MOND regime at large radii. When the mass M is much more extended than its transition radius, no special effects are expected at r_t . In this case the acceleration inside the body is smaller than a_0 and the system is everywhere in the deep MOND regime: there is no Newtonian-MOND transition anywhere. However, when the mass is well within its transition radius there is a marked change in the dynamics of test particles when crossing the transition region: the potential goes from $1/r$ to logarithmic; the rotation curve goes from Keplerian to flat, etc.. If we then look at the fictitious “dark matter” density distribution, or, as is done with lensing, at its projected surface density distribution, there may appear near this radius a pronounced feature in the form of a maximum. For an axisymmetric system aligned with the line of sight this shows as a “ring” of dark matter. All this occurs without there being any corresponding feature in the source (baryonic) distribution.

Physics is replete with similar examples in which a feature appears in some field quantity at a radius that is unrelated to a length-scale characterizing the source distribution of the field. As in our case, the radius of the feature depends on the strength of the source alone and on some constants appearing in the field equations. One example is the appearance of a horizon at the characteristic scale attached to a mass in relativity, which is introduced by c and M ; i.e., the gravitational radius MG/c^2 . The Bohr radius, r_B , as a mark of a transition from quantum behavior for $r < r_B$ to a classical one for $r \gg r_B$ is another. And in less fundamental examples: the Bondi radius in spherical accretion, which depends on the central mass and the ambient gas temperature; and the screening length for a charge Q in a plasma.

In this regard it is interesting to note that, because of the approximate equality $a_0 \sim cH_0$ (Milgrom 1983a), we can write

$$r_t \sim (R_s R_H)^{1/2}, \quad (1)$$

where R_s is the Schwarzschild radius of the mass, and $R_H = c/H_0$ is the Hubble radius. The transition radius is thus, approximately, the harmonic mean of these two horizon radii. It is then of the order of the Einstein radius for cosmological lenses, but is much larger for local ones.

Here we consider this interesting MOND phenomenon in more detail. It turns out that beside the obvious dependence on the mass distribution in the lens, the appearance of the

above feature depends sensitively on the behavior of the yet undetermined interpolating function of MOND around its transition region. We thus calculate the ring for different forms of this function.

Regarding the implications of their finding to MOND, Jee et al (2007) make the following statement: “The ringlike mass structure at $r = 0.4$ Mpc surrounding the dense core at $r \leq 0.25$ Mpc not traced by the cluster ICM nor by the cluster galaxies serves as the most definitive evidence from gravitational lensing to date for the existence of dark matter. If there is no dark matter and the cluster ICM is the dominant source of gravity, the MONDian gravitational lensing mass should follow the ICM, which, however, does not show any hints of such peculiar mass distribution.” Although many were quick to embrace this view, it is, in fact, quite baseless: such orphan rings of phantom dark matter (PDM) are formed naturally in MOND (as possibly in other modified dynamics theories). Although they tend to be overwhelmed by the underlying baryon distribution itself (as they would in the DM scenario proper), there are circumstances in which they can be observed directly (i.e., without subtracting the source distribution).

As regards the ring in Cl 0024+17, we find that it can be reproduced naturally with this MOND phenomenon. It will be exciting indeed (and ironical) if the ring discovered by Jee et al. turns out to be a direct image of the MOND transition region, akin to an image of an event horizon of a black hole as viewed via its lensing effect on background sources.

This is an opportunity to dispel a common misconception about MOND: it does not predict that the PDM distribution follows that of the (baryon) sources as stated, e.g., in the above quotation from Jee et al. and in the discussion of the implications of the bullet cluster for MOND (Clowe et al. 2006, and see Angus et al. 2007 for the MOND answer). An obvious counterexample is a baryonic thin disc, which is predicted to have both a PDM disc of finite mass (whose mass distribution does not follow that of the source disc) and an extended spheroid of PDM which clearly doesn’t follow the source distribution (Milgrom 2001). Another example is a simple system of several point masses, whose distribution of MOND PDM is very complex, with, among other things, numerous regions of negative PDM density (Milgrom 1986b) and a system of surfaces of maximum density (such as the shells we discuss here).

Jee et al. (2007) attribute the observed ring to an actual ring (in 3-D) of dark matter resulting from a collision of two sub-clusters along the line of sight. Famaey et al. (2007a) note that MOND has long been known to require that the cores of clusters be dominated by some form of as yet undetected matter (e.g., Gerbal et al. 1992, Sanders 1999, Aguirre, Schaye & Quataert 2001, Sanders 2003, Pointecouteau & Silk 2005, Angus Famaey & Buote 2007). Famaey et al. (2007a) considered, in particular, neutrinos as proposed by Sanders

(2003). They thus show that the explanation of Jee et al. can be adopted in the MOND framework without adding new ingredients. Angus et al. (2007) show that this as yet unseen matter also accounts for the observations of the bullet cluster (Clowe et al. 2006).

The explanation of the observed ring as a projection of the MOND PDM transition shell does not require, of course, a collision to have produced it. However, it is possible that such a collision has created a mass distribution that brings out the ring more clearly. We also find that, although it is not necessary, an aligned dumbbell configuration is more conducive to the detectability of a ring than a single spherical mass.

Our study here is by no means exhaustive; we only aim at demonstrating the phenomenon and studying in broad terms how it depends on the various inputs. In particular, we limit ourselves to some simple axisymmetric mass distribution that, in addition, are aligned with the line of sight. This applies to spherical systems in general, and also to the case of the cluster Cl 0024+17, which is believed to be an aligned double cluster.

In section 2 we lay out the basic ideas behind the appearance of “rings” in MOND. In section 3 we give the results for various axisymmetric systems and various forms of the interpolating function. In section 4 we consider the possible relevance to Cl 0024+17. Section 5 discusses the phenomenon in single galaxies. Section 6 is a discussion.

2. The phantom “dark matter” surface density: shells and rings

When studying the potential field of a mass distribution in MOND, it is sometime useful to describe it in terms of the added mass that would be required to produce the same field in Newtonian dynamics. This will remain useful as long as many continue to think in terms of dark matter. In the present nonrelativistic formulations of MOND as modified gravity, this phantom dark matter (PDM) density, ρ_p , is given by (Milgrom 1986b, 2001)

$$\rho_p = -(4\pi G)^{-1} \vec{\nabla} \cdot \mathbf{g} - \rho. \quad (2)$$

Here ρ is the actual (“baryon”) mass density, and $\mathbf{g}(\mathbf{r})$ is the MOND acceleration field. The first term in eq.(2) is the dynamical mass density, ρ_D , deduced using Newtonian dynamics.

Properties of the PDM distribution have been investigated in the past. For example, Milgrom (1986b) showed that the PDM density can be negative under certain circumstances; Brada and Milgrom (1999) showed that it cannot produce accelerations much exceeding a_0 no matter what the true density distribution is, and this was confirmed by Milgrom and Sanders (2005) for a sample of galaxies from rotation curve analysis; Milgrom (2001) studied the properties of the PDM halo of disc galaxies. Here we shall concentrate on another

property of the PDM halo and show that its density can have maximal surfaces in regions of space where no such features exist in the underlying source distribution ρ (they may, e.g., appear in vacuum). And when projected on the sky these surfaces lead to the appearance of line features such as rings or other ridge-like structures.

The total Newtonian dynamical mass of an isolated (bounded) mass is infinite as the MOND potential is asymptotically logarithmic in this case. However, in some sense we can say that two density distributions that have the same total (bounded) mass, also have the same total dynamical mass: Consider two density distributions ρ_1 and ρ_2 having the same total (true) mass, and both bound. Take a large volume ℓU of a fixed shape U but increasing linear dimension ℓ . Then the resulting dynamical (or phantom) mass distributions satisfy in the limit $\ell \rightarrow \infty$

$$\int_{\ell U} (\rho_{D,1} - \rho_{D,2}) d^3r \rightarrow 0. \quad (3)$$

This is because from eq.(2)

$$\int_{\ell U} (\rho_{D,1} - \rho_{D,2}) d^3r \propto \int_{\ell S} (\mathbf{g}_1 - \mathbf{g}_2) \cdot d\vec{\sigma}, \quad (4)$$

where S is the surface of U . And, Milgrom (1986a) has shown that next to the leading term at large radii, $-(MGa_0)^{1/2}\vec{r}/r^2$, which is common to \mathbf{g}_1 and \mathbf{g}_2 , there is a term (which may be angle dependent) that decreases as $r^{-(\sqrt{3}+1)}$, fast enough to make the limit of expression (4) vanish.

In the Lagrangian formulation, put forth by Bekenstein and Milgrom (1984), we have $\mathbf{g} = -\vec{\nabla}\phi$, where ϕ is the gravitational potential satisfying the modified, nonlinear Poisson equation

$$\vec{\nabla} \cdot [\mu(|\vec{\nabla}\phi|/a_0)|\vec{\nabla}\phi|] = 4\pi G\rho, \quad (5)$$

where $\mu(x)$ is the MOND interpolating function satisfying $\mu(x) \rightarrow 1$ for $x \rightarrow \infty$, and $\mu(x) \approx x$ for $x \rightarrow 0$. We shall, however use throughout the much more manageable approximation to this theory in which the MOND and Newtonian accelerations, \mathbf{g} and \mathbf{g}_N respectively, are algebraically related:

$$\mu(|\mathbf{g}|/a_0)\mathbf{g} = \mathbf{g}_N. \quad (6)$$

It is sometimes more convenient to work with the inverse of eq.(6) and define the interpolating function $\nu(y)$ (Milgrom 1986a) such that

$$\mathbf{g} = \nu(|\mathbf{g}_N|/a_0)\mathbf{g}_N. \quad (7)$$

The algebraic relation was the first formulation of the MOND paradigm, posited to apply for test particle motion (Milgrom 1983a). It is an exact consequence of the Lagrangian

formulation, for example, for spherical systems and it captures the salient consequences of the Lagrangian formulation in other configurations. At any rate it is good enough for our demonstrative purposes here. Note that $\mu(x) = 1/\nu(y)$, where $x = g/a_0$, and $y = g_N/a_0$, and that $\nu(y) \rightarrow 1$ for $y \rightarrow \infty$ and $\nu(y) \rightarrow y^{-1/2}$ for $y \rightarrow 0$.

The phenomenon discussed here may be studied with massive test particles, as in rotation-curve analysis. But, since the present motivation comes from lensing, we discuss the phenomenon in terms of its appearance in lensing analysis: we present the results in the form of the projected surface density derived from ρ_p , or of that of the total dynamical mass density ρ_D .

In calculating lensing in MOND we assume that it is given by the standard general relativistic formula using the non-relativistic MOND potential, which governs the motion of massive test particles. This recipe follows from TeVeS (Bekenstein 2004), the best relativistic formulation of MOND we have at present.

As in Milgrom (1986a), we exploit the scaling relations of the MOND equations (both formulations enjoy the same relations) and use henceforth dimensionless quantities: Our unit of mass will be M , the total true (“baryonic”) mass of the system; the unit of length is the transition radius, $r_t \equiv (MG/a_0)^{1/2}$. All other units are formed from them: that of acceleration is $MG/r_t^2 = a_0$; that of the gravitational potential is $a_0 r_t = V_\infty^2 = (MGa_0)^{1/2}$; that of density is Mr_t^{-3} ; and that of surface density is $\Sigma_0 \equiv Mr_t^{-2} = a_0/G$. In these units G and a_0 disappear from the above MOND equations. Note that unlike the units of other quantities, which depend on the total mass, those for acceleration and surface density are universal constants. This fact underlies the results of Brada and Milgrom (1999) and also our results here showing that Σ_0 is always the characteristic surface density of the PDM in the region of the feature. Note also that because of the nearness of a_0 to cosmological acceleration (Milgrom 1983a) Σ_0 is also on the order of the critical lensing surface density for objects at cosmological distance (Sanders 1999).

It is easy to understand why ρ_p , and hence possibly also ρ_D , may possess a shell-like feature: This occurs when the mass in the system is well contained within its transition radius. Let us consider, heuristically, a point mass, and assume a MOND interpolating function of the form that crosses abruptly from one asymptotic regime to the other:

$$\mu(x) = \begin{cases} 1 & : x \geq 1 \\ x & : x < 1 \end{cases} . \quad (8)$$

Then, for all radii smaller than 1 the accelerations are in the Newtonian regime, and no PDM is predicted there. Beyond $r = 1$ we have already deep MOND behavior; so, ρ_p jumps to $1/4\pi$ at $r = 1$ and hence outward $\rho_p = 1/4\pi r^2$: a shell in the PDM distribution. The

corresponding projected surface density that will be deduced from standard GR lensing in this case is:

$$\Sigma(R) = \frac{\pi}{2} \Sigma(0) R^{-1} \begin{cases} 1 - \frac{2}{\pi} \arctan[(R^{-2} - 1)^{1/2}] & : R \leq 1 \\ 1 & : R > 1 \end{cases}, \quad (9)$$

where the central value $\Sigma(0) = 1/2\pi$, and R is the projected radius.

Thus $\Sigma(R)$ (for the PDM alone) starts at $1/2\pi$ at the center, increases to $1/4$ at $R = 1$ and beyond it declines as $1/4R$. This is the “ring” we speak of. This example already demonstrates the salient properties of the ring in the more general (axisymmetric) cases: The ring appears at a radius of order 1, has a maximum surface density of order (usually somewhat smaller than) 1, and has a contrast of that order.

Because the appearance of the shell feature is contingent on the transition from the Newtonian regime to the MOND regime, its exact properties depend strongly on the behavior of the transition function $\mu(x)$ near $x = 1$. This is also true of the exact maximum acceleration the PDM can create as discussed in Brada and Milgrom (1999) (the two phenomena are related). If such MOND rings are clearly identified in enough systems this may provide important constraints on the form of μ in the transition region. As part of our study we consider various forms of μ . We next discuss this function in more detail.

2.1. The MOND interpolating function

In modified inertia formulations of MOND it is not clear that there is one transition function that characterizes all motions, although such a function does appear universally in the description of circular motions in axisymmetric potentials (Milgrom 1994). From this it would follow that a shell in the PDM distribution as deduced from rotation curve analysis, but not necessarily lensing analyses, is expected also in modified inertia formulations of MOND. In fact, given the sensitivity of the appearance of the ring to the form of the interpolating function, the ring may well have a different location or amplitude in lensing vs. rotation curve analysis in the context of modified inertia formulations (this could possibly distinguish between modified gravity and modified inertia). However, such formulations are not yet developed enough to tell us what to expect when probing the potential field with non circular motions (such as lensing). So, here we base our discussion on modified gravity formulations, in which, generically, an interpolating function appears. For example, in the above Lagrangian theory, the Lagrangian density of the gravitational potential is $\propto F[(\vec{\nabla}\phi)^2/a_0^2]$, and $\mu(x) \propto dF(x^2)/d(x^2)$.

We consider representatives from three one-parameter families of interpolating functions: The first is

$$\mu_\alpha(x) = \frac{x}{(1+x^\alpha)^{1/\alpha}}, \quad (10)$$

with the corresponding

$$\nu_\alpha(y) = \left[\frac{1 + (1+4y^{-\alpha})^{1/2}}{2} \right]^{1/\alpha}. \quad (11)$$

The case $\alpha = 2$ has been extensively used in rotation curve analysis from the first analysis by Kent (1987), through Begeman Broeils and Sanders (1991), and to this day. The choice μ_1 has been used occasionally in various analyses (e.g. Milgrom 1986a) and has recently been suggested to perform better than μ_2 in rotation curve analysis (Zhao and Famaey 2006, Sanders and Noordermeer 2007). Famaey and Binney (2005) found that neither μ_1 nor μ_2 adequately fit the rotation curve of the Milky Way with its Basel mass model (Bissantz, Englmaier and Gerhard 2003); a good fit is achieved for a function that is near μ_1 for small arguments but approaches μ_2 at high arguments. The limiting case, eq.(8), corresponds to very large α . Moreover, where $y \rightarrow \infty$, $\nu_\alpha \approx 1 + y^{-\alpha}/\alpha$; for $y \rightarrow 0$, $\nu_\alpha \approx y^{-1/2} + y^{(\alpha-1)/2}/2\alpha$.

The second and third families, which we consider here for the first time, are defined by their inverse, or $\nu(y)$, functions:

$$\tilde{\nu}_\alpha(y) = (1 - e^{-y})^{-1/2} + \alpha e^{-y}, \quad (12)$$

with its corresponding $\tilde{\mu}_\alpha(x)$, and

$$\bar{\nu}_\alpha(y) \equiv (1 - e^{-y^\alpha})^{(-1/2\alpha)} + (1 - 1/2\alpha)e^{-y^\alpha}, \quad (13)$$

with the corresponding $\bar{\mu}_\alpha$. At small y this third family goes as $y^{-1/2} + y^{\alpha-1/2}/4\alpha + 1 - 1/2\alpha$. The choice of α permits a very fast transition to the Newtonian regime near $y = 1$.

These choices do not follow from any physical considerations. [In fact, at present, we know of no concrete theoretical considerations that can dictate the form of $\mu(x)$.] They do not even span the whole range of possibilities. We only use them to show the variety that is possible and to demonstrate the sensitivity of the ring phenomenon to the exact choice.

There are some constraints on the interpolating function: $\mu \rightarrow 1$ for $x \rightarrow \infty$ is dictated by Newtonian correspondence (although the way in which μ approaches 1 is not known, but enters crucially into phenomena such as solar system effects). The limit $\mu \rightarrow x$ for $x \rightarrow 0$ is dictated by the basic premises of MOND (it insures asymptotically flat rotation curves for isolated systems). Another requirement is that $\hat{\mu}(x) \equiv d\ln(\mu)/d\ln(x) > -1$ everywhere. This is the ellipticity condition for the Lagrangian theory field equation. It is tantamount to the sign definiteness of the Hessian of the Lagrangian as a function of the components of

$\vec{\nabla}\phi$) and insures uniqueness of the solution under the Dirichlet and/or Neumann boundary condition (e.g. Milgrom 1986a). This condition also says that $x\mu(x)$ [and equivalently $y\nu(y)$] is a monotonic function, which is required for the above algebraic relation, eqs.(6)(7), between \mathbf{g} and \mathbf{g}_N to have a unique solution. Beyond this requirement the form of μ is free at the moment and we can only hope to use the data to constrain it.

Zhao and Famaey (2006) have pointed out that in the formulation of TeVeS in Bekenstein (2004) the effective interpolating function $\mu_e(x)$ has to approach 1 rather slowly in the high acceleration limit. Their argument is best paraphrased in terms of the ν function: If ν is that of the scalar field in TeVeS, then $\nu_e(y) = \nu(y) + 1$ is the effective function for the full gravity. At small y , $\nu \approx y^{-1/2}$ as dictated by MOND, so $y\nu(y)$ is increasing there. But the ellipticity condition says that $y\nu(y)$ has to be a monotonic function; so it must remain increasing, and hence ν cannot vanish faster than a/y at large y . So, in turn, ν_e cannot approach 1 faster than that. Since $\mu(x) = 1/\nu(y)$, and for $y \gg 1$ $x \approx y$, it follows that also $\mu(x)$ has to approach 1 no faster than a/x (see also Famaey et al. 2007b for a discussion of this constraint and for ways to relax it). None of the interpolating functions considered above satisfy this requirement except for μ_1 . We, however, ignore this kind of constraint. It is exactly this behavior that potentially gets TeVeS in trouble with solar system and binary pulsar constraints (see e.g. the detailed discussion in Bruneton and Esposito-Farese 2007). So, a working version of TeVeS may well have to have this aspect of it expurgated. It may be possible to dispose of this constraint altogether by considering a theory with other potentials. For example the relativistic version of Zlosnik Ferreira & Starkman 2007 doesn't seem to require this behavior. From a theoretical point of view, there remains complete freedom to choose the form of μ so long as the basic constraints outlined above or satisfied.

We show in Fig. 1 the forms of μ , ν , and the Lagrangian function $F(z)$ for two choices of the parameter in each family. We see that for $\tilde{\mu}_\alpha$ and $\bar{\mu}_\alpha$ the approach to 1 can be as gradual as μ_1 in the MOND regime, but then with a rather more rapid transition when $a/a_0 > 1$.

We can classify the interpolating functions according to several attributes: how fast $\mu(x)$ approaches 1 for very high values of x (this is important for calculating the MOND correction in highly Newtonian systems, such as the solar system, and is not crucial here); how far $\mu(x)$ stays near 1 as x approaches $x = 1$ from above; how fast $\mu(x)$ departs from the initial $\mu \sim x$ at low values of x . All of the attributes affect the appearance of the ring at r_t , and within each of the one-parameter families it is that one parameter that controls all aspects. To be able to explore the different attributes separately we consider these three families.

To demonstrate the ability of rotation curve analysis to discriminate between the inter-

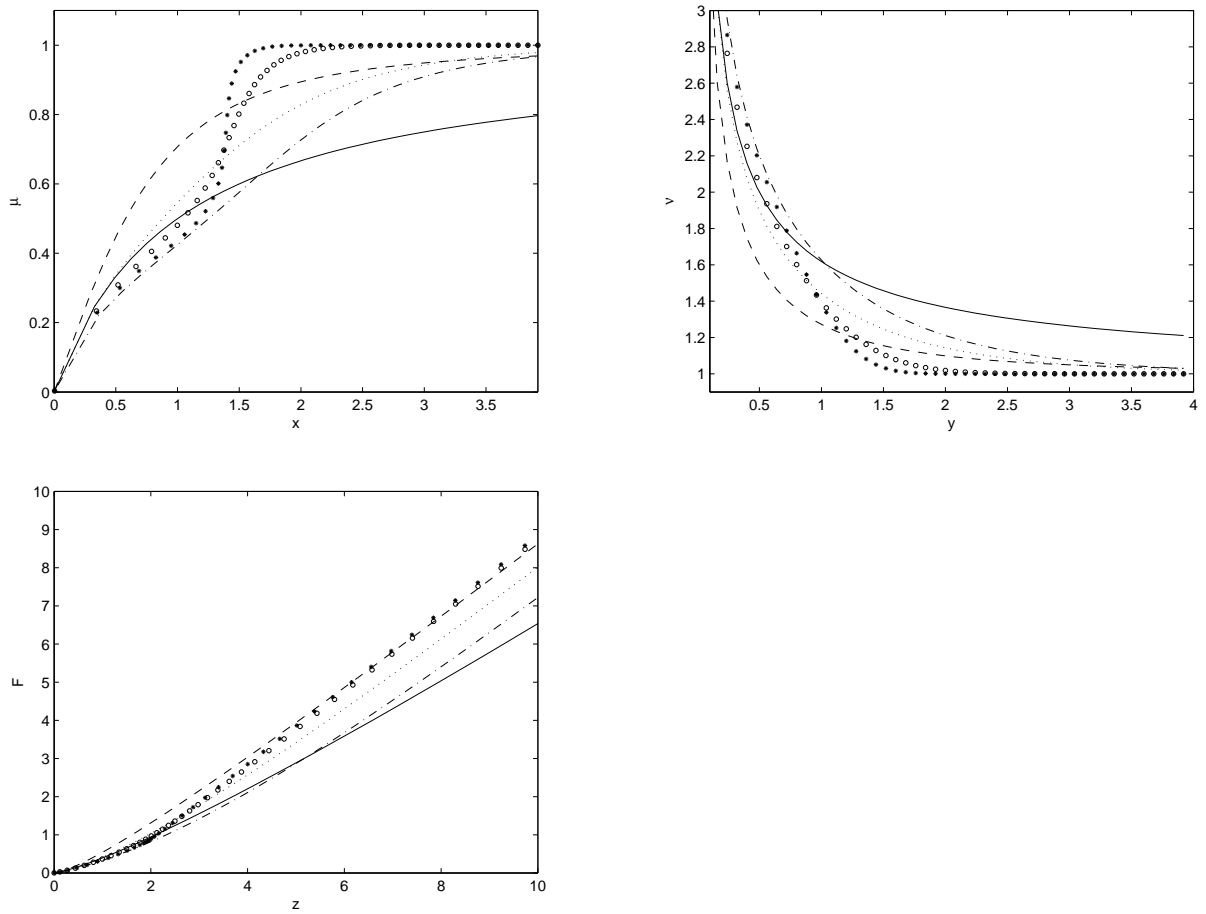


Fig. 1.— The form of $\mu(x)$, $\nu(y)$, and the Lagrangian function $F(z)$ for μ_1 (solid), μ_2 (dashed), $\tilde{\mu}_{0.5}$ (dotted) $\tilde{\mu}_1$ (dash-dot), $\bar{\mu}_2$ (circles) and $\bar{\mu}_3$ (stars).

polating functions, we show in Fig. 2 the rotation curves for a pure exponential disc and pure de Vaucouleurs sphere of different scale lengths and for different choices of the interpolating function. We see that with the more extreme forms in our sample one even expects to see an orphan feature directly in the rotation curve of galaxies with high enough surface densities, or mean acceleration. (An orphan feature is one that is not directly dictated by the underlying source distribution and hence does not appear on the Newtonian rotation curve.) A more systematic study of this point is required to insure that we adopt a form of μ that is compatible with rotation curve analysis (and see section 5 for a beginning of such analysis). We reemphasize, however, that the forms of μ we use here are not suggested as real candidates. We chose them essentially to span some range of behaviors so that we can demonstrate the dependence of the ring phenomenon on μ , although some of the new forms of μ do seem to do better for high acceleration galaxies (see section 5) as well as being more favorable for the visibility of the "ring".

2.2. Structure along the line of sight

The thin-lens approximation, so useful in conventional dynamics, does not apply in MOND : Because of the inherent nonlinearity of MOND, even in the nonrelativistic limit, two ("baryonic") mass distributions having the same projected surface density distributions for a given line of sight, do not, in general, have the same surface densities of the corresponding PDM (Mortlock and Turner 2001, Milgrom 2002). For example, as explained in Milgrom (2001) N equal masses well separated along the line of sight produce, in the deep MOND regime, a deflection angle, for a given impact parameter, that is \sqrt{N} times larger than when the N masses are melded in one. Such effects will be clearly shown by our numerical results below.

It should be emphasized that for gravitational lensing in a theory such as TeVeS, the relation between the deflection of photons and the total weak field force is the same as that in General Relativity. This means that the surface density derived for the PDM (using, for example, the lens convergence estimated from the observed shear) is identical to that obtained by integrating the density of the PDM along the line of sight.

The discussion above eq.(3) tells us that for two mass distributions of the same total (true) mass we have

$$\int_0^R [\Sigma_1(R') - \Sigma_2(R')] R'^2 dR' \rightarrow 0, \quad (14)$$

in the limit $R \rightarrow \infty$.

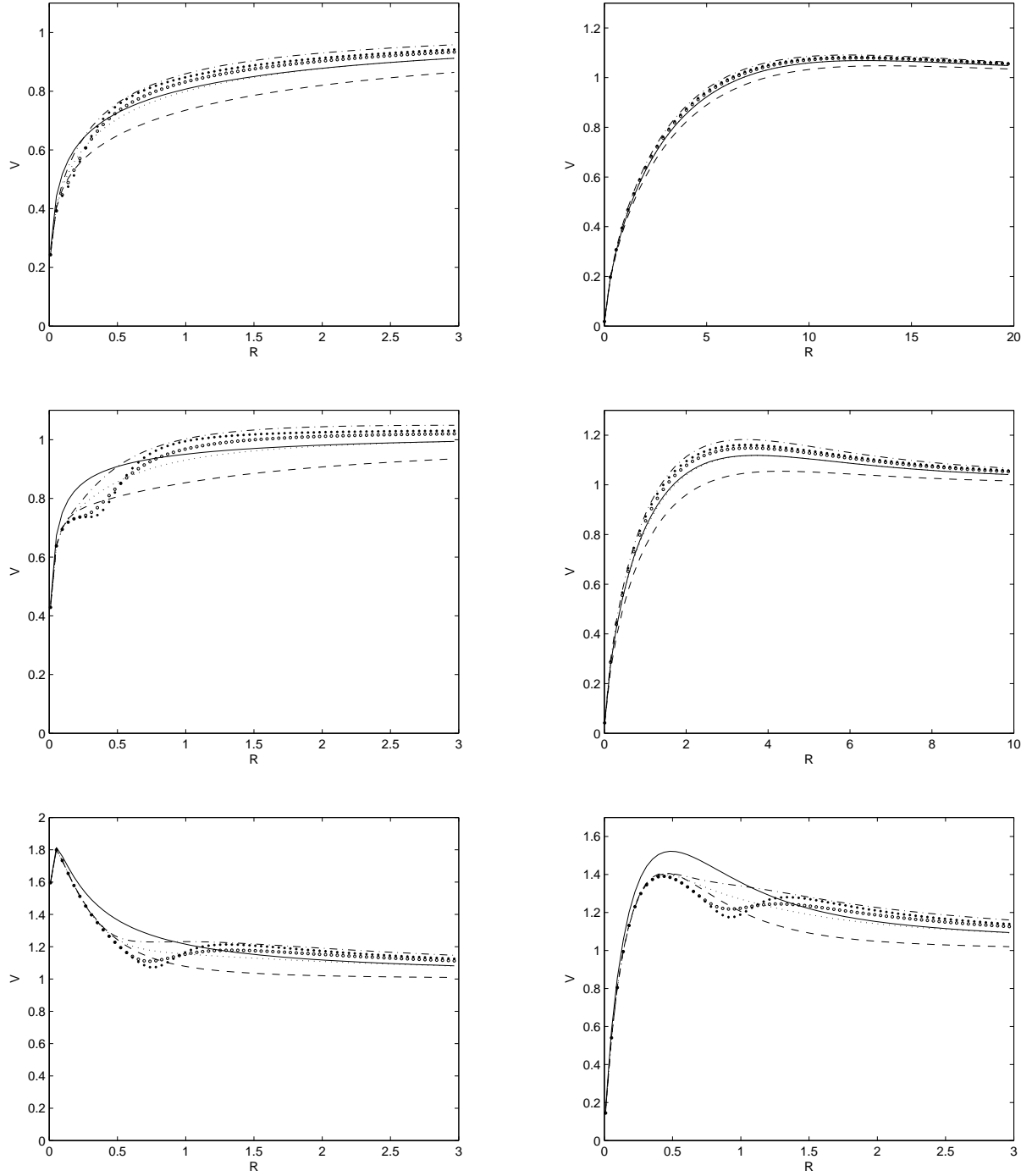


Fig. 2.— MOND rotation curves for de Vaucouleurs spheres (left) and exponential discs (right). The former (from top to bottom) for effective radii 2, 1, $1/6$ (all in units of the transition radius); the latter (from top to bottom) for scale lengths 3, 1, $1/5$. The different curves are for different interpolating functions: μ_1 (solid), μ_2 (dashed), $\tilde{\mu}_{0.5}$ (dotted), $\tilde{\mu}_1$ (dash-dot), $\bar{\mu}_2$ (circles) and $\bar{\mu}_3$ (stars).

3. Examples

3.1. Spherical lenses

Here we discuss the simple case of a spherical lens represented by a point mass; so that our results can be applied directly everywhere outside any spherical mass. In this case, since $g_N = r^{-2}$, we have

$$4\pi\rho_p = r^{-2} \frac{d(r^2 g)}{dr} = r^{-2} \frac{d[\nu(r^{-2})]}{dr} = -2\nu'(r^{-2})r^{-5}. \quad (15)$$

We show in Fig. 3 the surface density of the PDM for a point mass with different choices of μ . We see that the occurrence of a maximum leading to the appearance of a ring is rather generic. Of all the choices of μ shown in the figure a maximum at a finite radius does not appear only for μ_1 and $\mu_{3/2}$. This is easy to understand: For this form of μ we have in the high acceleration limit $g \approx g_N + \alpha^{-1}g_N^{(1-\alpha)}$. Since $g_N \propto r^{-2}$, we have $\rho_p \propto r^{2\alpha-3}$. So for $\alpha \leq 3/2$ there is no “hole” in the PDM density, and a maximum can appear only for $\alpha > 3/2$. We also see that the radius (in units of r_t), the height, and the contrast of the maximum depend rather sensitively on the properties of the interpolating function. The location of the peak is controlled mainly by the approximate x value at which $\mu(x)$ approaches 1 (in the vicinity of $x = 1$, not in the far asymptotic regime). So, for example, the limiting case μ_∞ produces a maximum at $r = 1$, which is the largest for all the functions we study here. For the other forms of μ we use it goes near a value of 1 for $x > 1$; accordingly, the ring occurs at $r < r_t$. The height of the peak is sensitive to how low $\mu(x)$ stays for values of $x < 1$. With this guidelines one can construct μ forms to engineer the ring properties. To recapitulate, the formation of the apparent ring is generic if the mass is centrally condensed with respect to r_t . It is not produced only for some special forms of μ such as μ_α with $\alpha \leq 3/2$.

3.2. Aligned dumbbell lenses

Here, for simplicity, we still use the algebraic relation, eqs.(6)(7), even though it is not exact anymore. We show in Fig. 4 the predicted surface density of the PDM for two equal point masses aligned with the line of sight for different separations, and different choices of the interpolating function. Figure 4 [together with Fig.(5)] demonstrates clearly that the thin-lens approximation is not valid in MOND as all the mass models it describes have the same projected (baryonic) mass. They all give the same result at radii much larger than the separation (where they all act like a point mass); but at smaller radii elongation of the mass along the line of sight enhances the lensing signal (see Milgrom 2002). When the separation

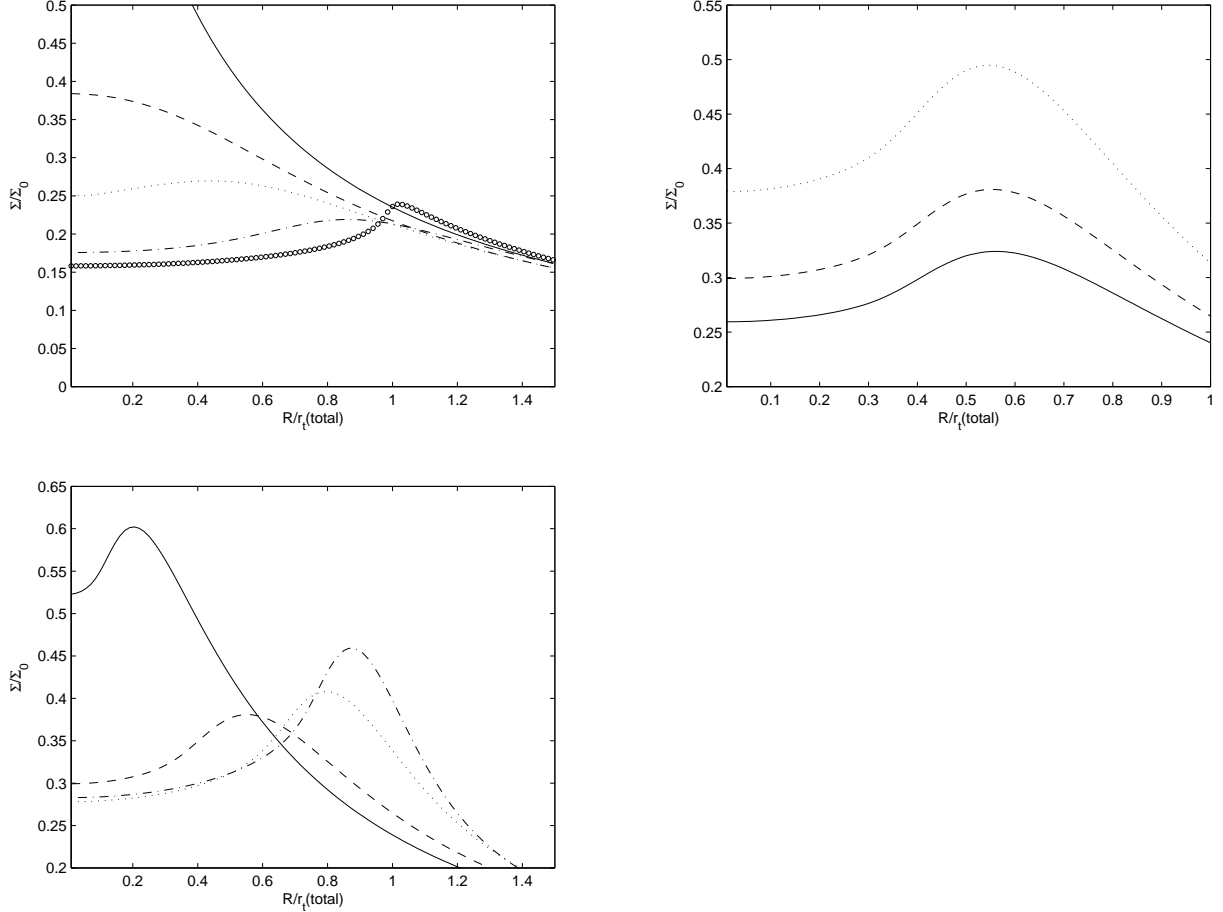


Fig. 3.— The MOND predicted PDM surface density, in units of Σ_0 , for a point mass with different forms of the MOND function. Top left: μ_α with $\alpha = 1, 3/2, 2, 4, 50$ (the higher α the lower Σ at low radii). Right: $\tilde{\mu}_\alpha$ with $\alpha = 0.25, 0.5, 1$ (the higher α the higher Σ). Bottom left: $\bar{\mu}_\alpha$ with $\alpha = 0.5$ (solid), $\alpha = 1$ (dashed), $\alpha = 2$ (dotted), $\alpha = 3$ (dot-dash).

is much smaller than 1 (the individual transition radius) the system acts like one point mass of value 2, whose transition radius is thus $2^{1/2}$; however, as regards the normalization, the resulting surface density of the PDM is the same as that of a single mass (as this does not depend on the mass). In the other extreme, when the separation is much larger than 1, the PDM surface density is simply double that of a single mass in magnitude, and it has the same radial distribution. This is also in line with relation (14).

For brevity's sake we show only results for equal masses. Clearly, with unequal masses a more complex profile results, with possibly two maxima.

Note that for some separations and some forms of μ , the PDM surface density profile shows an upturn towards small radii. This is another orphan feature of MOND connected with the vicinity of the point where $g = 0$.

3.3. A thin mass rod along the line of sight

Consider a mass M of constant density, with diameter D and length L aligned with the line of sight. Assume that $D/2 \ll r_t = (MG/a_0)^{1/2}$ (we shall take $D = 0$). For there to be an enhanced effect over a point mass we have to have $L \gg r_t$, then the mass will act roughly like $N = L/r_t = (MG/L^2a_0)^{-1/2}$ separate masses each of value $m \equiv M/N$. The effect of increasing N is thus to bring closer the radius of the maximum and at the same time raise its height, also in line with eq.(14).

Again, taking as an example the μ_α family, in the high acceleration limit we have $g \approx g_N + \alpha^{-1}g_N^{(1-\alpha)}$. For small N we are basically still in the point mass limit. But for large N , when we are near the mass, the field is approximately that of an infinite wire; so $g_N \propto r^{-1}$. We then have $\rho_p \propto r^{\alpha-2}$; so, now the limiting value of α (for getting a "hole") for large N is $\alpha = 2$.

We show in Fig. 5 the projected phantom surface density for different values of N and for various interpolating functions.

4. Possible relevance to Cl 0024+17

Jee et al. (2007) offer an explanation of the apparent ring in Cl 0024+17 in terms of an actual ring of dark matter, in 3-D, produced by a past collision of two clusters occurring along the line of sight. The two clusters are now separated from each other. Jee et al. adduce cogent evidence to show that the cluster is indeed composed of (at least) two separate

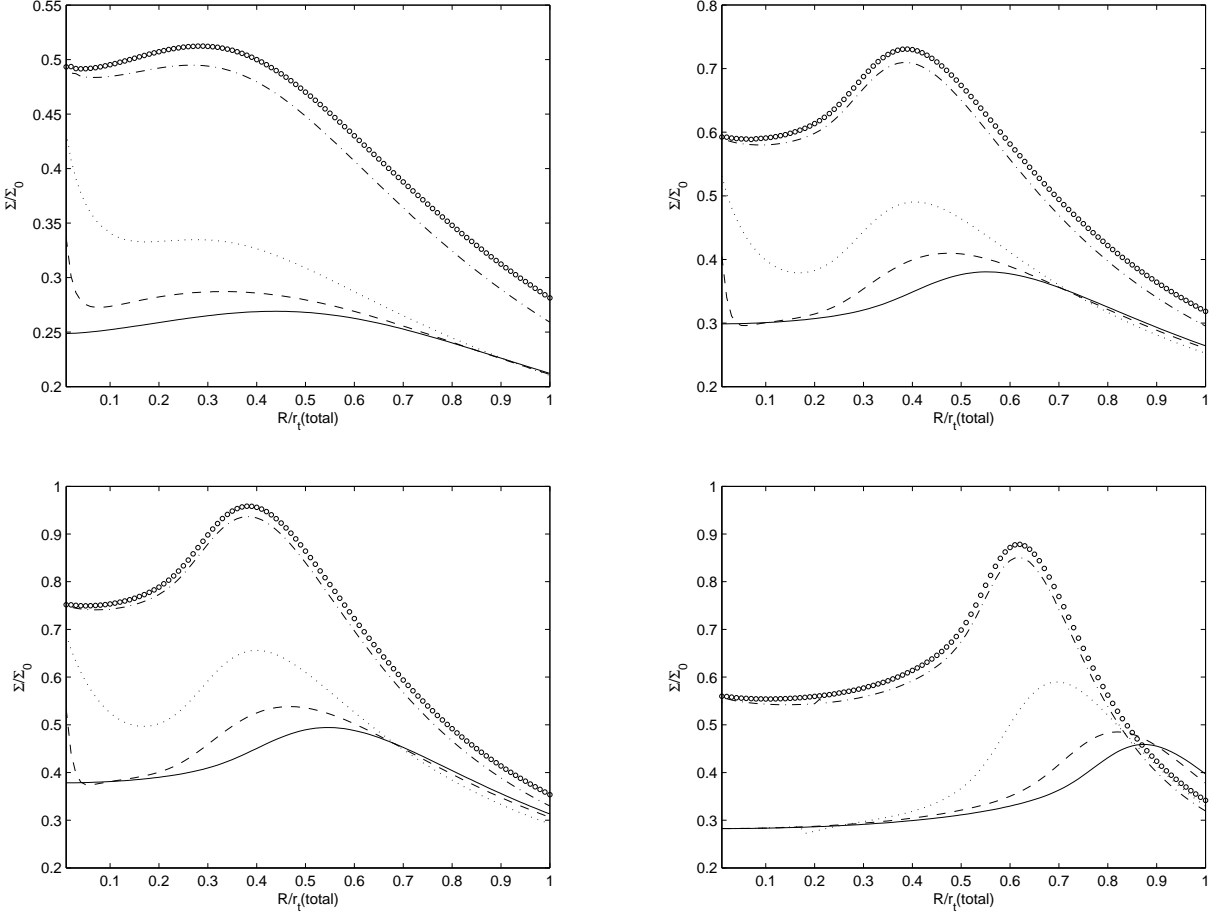


Fig. 4.— The MOND predicted PDM surface density, in units of Σ_0 , for two equal point masses along the line of sight separated by 0 (solid), 0.5 (dashed), 1 (dotted), 4 (dashed-dotted), 20 (circles) transition radii for the total mass. For μ_2 (upper left), $\tilde{\mu}_{0.5}$ (upper right), $\tilde{\mu}_1$ (lower left), and $\bar{\mu}_3$ (lower right).

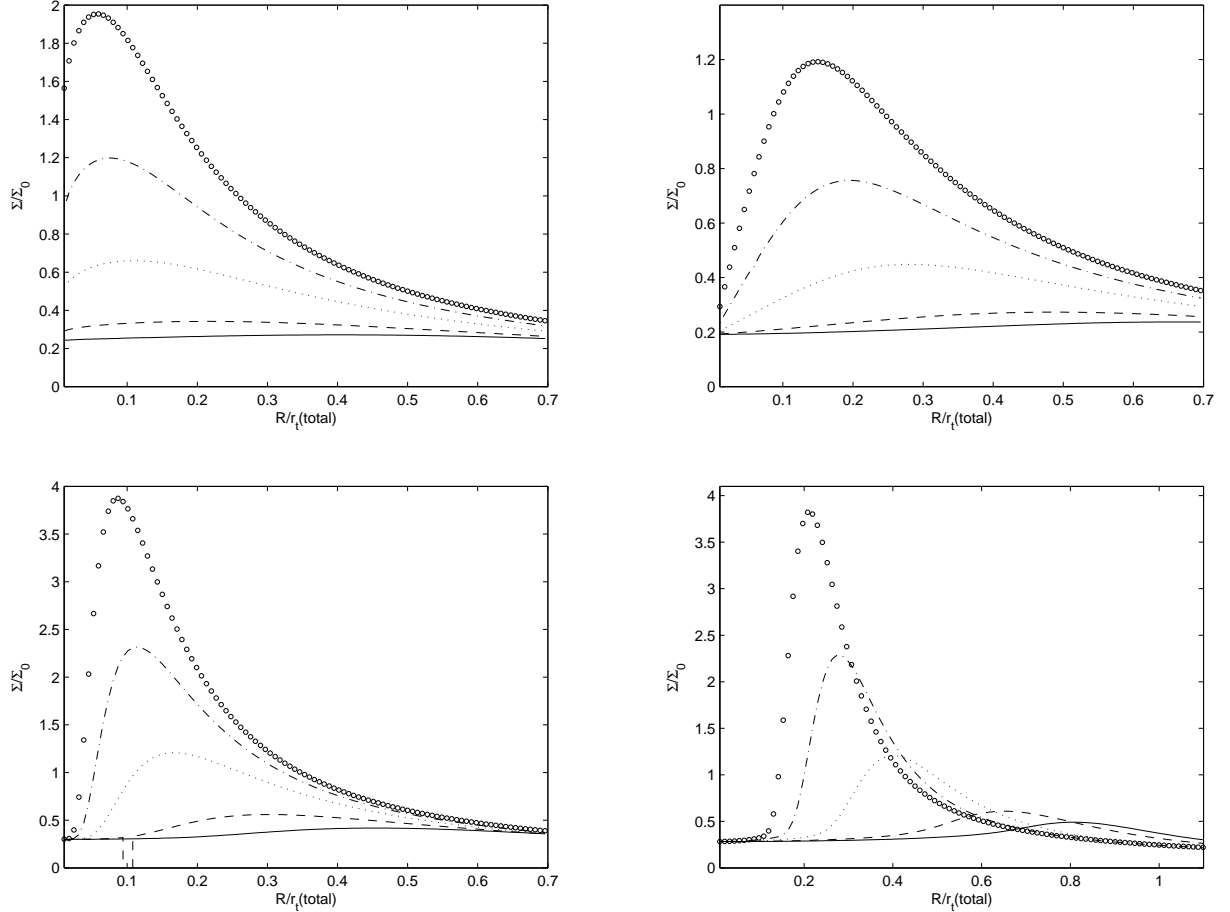


Fig. 5.— The MOND predicted PDM surface density, in units of Σ_0 , for a line mass of different lengths $N = 1, 2, 4, 6, 8$ (in units of the transition radius; higher peak Σ for higher N). Different interpolating functions are used: $\mu_{2.2}$ (top left), μ_3 (top right), $\tilde{\mu}_{0.5}$ (bottom left), and $\bar{\mu}_3$ (bottom right).

structures along the line of sight (bi-modality of the galaxy velocity distribution, and a factor-of-2 discrepancy between the masses deduced from X-ray analysis and from weak lensing). Famaey et al. (2007a) give a similar explanation in the framework of MOND building on the fact that MOND too requires DM in the cores of clusters. The past collision is a necessary ingredient in these explanations. Our mechanism depends only on the present mass distribution and cares little as to whether or not there occurred a collision in the system. (Although in some unknown way the collision could have created a special mass distribution that is expedient to a ring formation.)

As stated above, galaxy clusters are required to contain large quantities of as yet undetected matter, even in the context of MOND. Direct observations thus do not tell us how much conventional (MOND source) matter there is in the cluster and how it is distributed. In addition, as we explained above, the actual distribution of that mass in 3-D is very crucial, and this can certainly not be deduced from the observations. For these reasons, and because we do not know the exact form of the interpolating function, we are not in the position to construct a specific model for the ring in Cl 0024+17 (Jee et al. also do not have a specific model only a plausibility scenario, as the required details of the underlying collision are not known). Instead, we want to see only if the observed parameters of the ring can naturally result from the mechanism that we discuss here.

The surface density distribution deduced by Jee et al. (2007) is unusual for single clusters: It is characterized by a very concentrated component followed by an almost constant surface density out to the last measured point; the ring appears on the background of this plateau. As stated above it is the fact that there is a central concentrated component that is conducive to ring appearance.

There are four observables that we want to reproduce in rough terms: the radius at the ring maximum, the mass within that radius, the surface density at the location of the maximum, and the contrast of the ring. Jee et al. give the radius of the ring (presumably that of the maximum) as 400kpc (75''). According to our previous results this should be some fraction of the transition radius. So r_t would be typically between 500kpc (if $r/r_t = 0.8$) and 1600kpc if ($r/r_t = .25$). We have

$$r_t = 833(M/5 \times 10^{14}M_\odot)^{1/2}(a_0/10^{-8} \text{ cm s}^{-2})^{-1/2}\text{kpc}, \quad (16)$$

so the required (projected) mass inside the ring would be somewhere between $2 \times 10^{14}M_\odot$ and $20 \times 10^{14}M_\odot$. This are only rough estimates but they do define the right ballpark, as the projected dynamical mass within the radius of the maximum, according to Fig. 12 of Jee et al., is $\sim 8 \times 10^{14}M_\odot$ and that within the observed minimum (at 50'') is $\sim 4 \times 10^{14}M_\odot$.

The critical surface density with respect to which Jee et al. plot their deduced surface densities: $\Sigma_c = c^2(4GD)^{-1} = 0.35 \text{ g cm}^{-2} (D/1\text{Gpc})^{-1}$, where $D = D_d D_{ds}/D_s$; the D s are angular diameter distances to the lens (d), the source (s), and between the two (ds). Jee et al. use for the fiducial red-shift of the source $z = 3$. We take $D_{ds} \sim D_s$, and deduce D_d by noting that they quote the radius of the ring as $400\text{kpc} = 75''$. This gives $D \approx 1.1\text{Gpc}$. So $\Sigma_c \sim 0.32 \text{ g cm}^{-2}$. Since $\Sigma_0 \sim 0.15 \text{ g cm}^{-2}$ (for $a_0 = 10^{-8} \text{ cm s}^{-2}$), $\Sigma_c \approx 2\Sigma_0$. Jee et al. find at the location of the ring $\Sigma \sim 0.7\Sigma_c \sim 0.22 \text{ g cm}^{-2} \sim 1.5\Sigma_0$. From Fig. 10 of Jee et al. we read for the ring contrast a difference between minimum and maximum of $\sim 0.06\Sigma_0$. This is rather easy to achieve.

As examples of configurations that roughly reproduce the Jee et al. parameters we show in Fig. 6 the total projected mass density of simple models for a few (favorable) forms of the interpolating function. These are not generic but were constructed to demonstrate that MOND can reproduce an observed surface distribution like the one observed.

Concentrating on the dumbbell results in the upper Fig. 6 we see that Σ values comparable with those deduced by Jee et al. can be achieved. Identifying the positions of the peak in the case of this dumbbell in Fig. 6 ($0.585r_t$, and $0.65r_t$ for $\bar{\mu}_2$ and $\bar{\mu}_3$ respectively) with that observed (400kpc) gives the total true (MOND) mass of the dumbbell as $3.4 \times 10^{14}\text{M}_\odot$, and $2.7 \times 10^{14}\text{M}_\odot$, respectively. According to our calculations, the integrated, projected Newtonian dynamical mass (true plus phantom) within the minimum in the above models is about 1.4 times the true source mass; so, in absolute terms it comes out to $\sim 4.8 \times 10^{14}\text{M}_\odot$, and $3.8 \times 10^{14}\text{M}_\odot$, respectively, to be compared with $4 \times 10^{14}\text{M}_\odot$, which Jee et al. find within the minimum. Mind you though that these are only indicative figures. We also emphasize that the true (MOND) mass we require is still much larger than the observed mass in gas and stars. From the β model fit of Zhang et al. (2005), we estimate the gas mass within a projected radius of 400 kpc to be $\sim 2.5 \times 10^{13}\text{M}_\odot$; the total mass of stars and gas together could be as large as $\sim 4 \times 10^{13} \text{ M}_\odot$ (although it is difficult to estimate the actual gas mass in this presumably double system). Therefore, as in other clusters, MOND still requires a significant quantity of undetected matter in the core (Sanders 2007). But the “ring” is not made of this, of course.

Finally, we note that there are other mass configurations that can achieve the same apparent surface density distribution; for example, take the single sphere case in Fig. 6 on the background of a constant-surface density distribution along the line of sight.

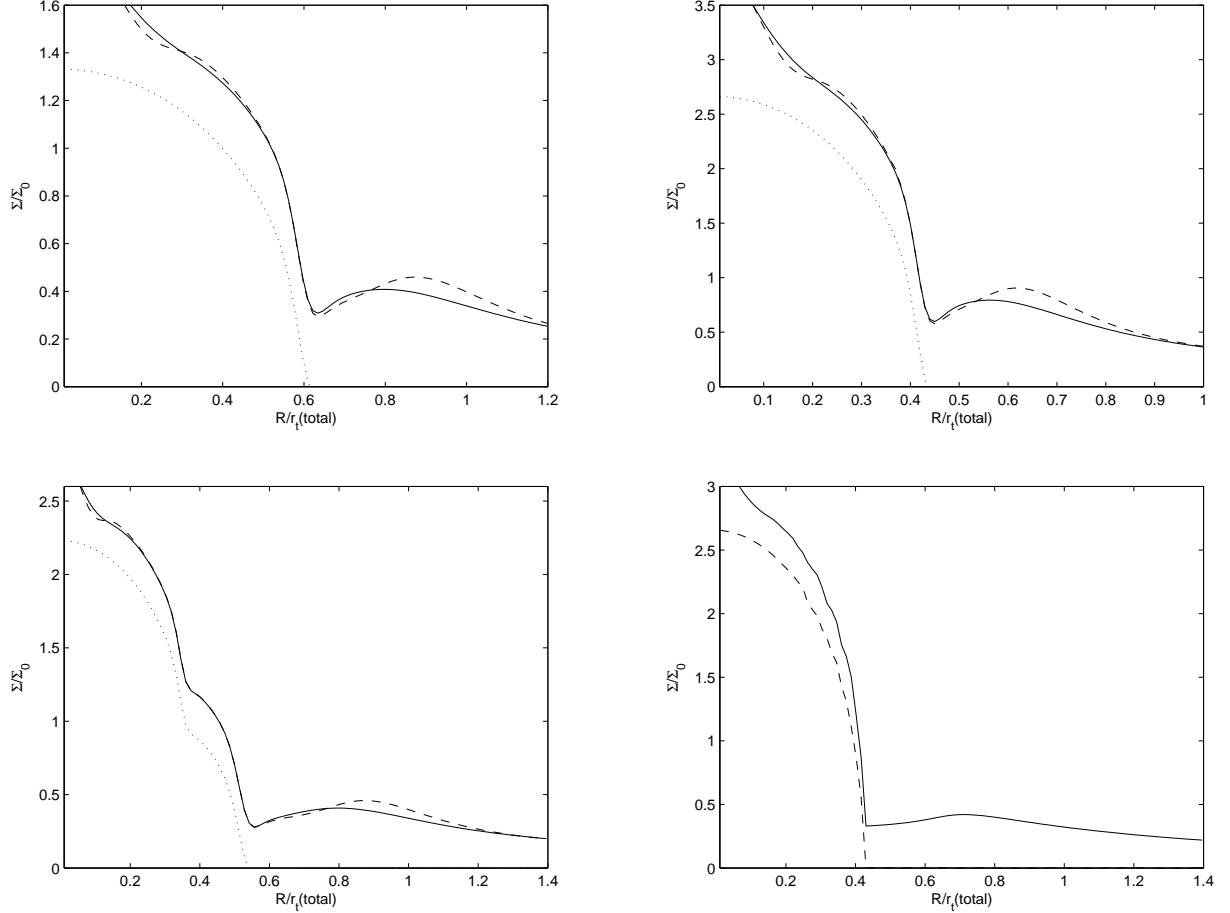


Fig. 6.— The total projected Surface density in units of Σ_0 . Upper left: for a single sphere of constant density with a radius that is 0.6 the transition radius. Upper right: for two spheres of constant density far apart from each other along the line of sight, each has a radius that is 0.6 of its own transition radius. Lower left: for two concentric spheres of constant densities of masses 1 and 0.3 and radii 0.53 and 0.35 of the total transition radius. All these for two interpolating functions: $\bar{\mu}_2$ (solid) and $\bar{\mu}_3$ (dashed). In each case the baryon contribution alone is shown as the dotted line. Lower right: a dumbbell of two equal spherical masses of constant density far apart along the line of sight with μ_{10} (the source, baryon, contribution in dashed line). For Cl 0024+17 the shear is $\kappa \approx 0.5\Sigma/\Sigma_0$.

5. Shells and rings in galaxies

The present discussion was prompted by the observation of a ring in a galaxy cluster. But, of course, the MOND orphan, transition feature may appear in various ways also in high surface brightness (HSB) galaxies. A galaxy is dubbed HSB in the MOND sense if its surface brightness is so high that the parameter $\xi \equiv (MG/\ell^2 a_0)^{1/2} = r_t/\ell \gg 1$, where ℓ is the scale length of the galaxy, say the half light radius for an elliptical galaxy, or the exponential scale-length of a disc. In this case the bulk of the baryonic mass is contained within the transition radius and there is then a good chance for the appearance of a pronounced feature. In fact, there is already evidence that in some HSB galaxies the PDM distribution has a hole surrounding the center of the galaxy. For example, this is the case for the Milky Way itself (Bissantz, Englmaier & Gerhard 2003). It has also been shown to apply to some elliptical galaxies (Romanowsky et al. 2003, Milgrom & Sanders 2003). To demonstrate the expectations from one of the galaxies in the study of Romanowsky et al. (2003), we show in Fig. 7 the projected surface density of the PDM alone and of the total for a de Vaucouleurs sphere with $\xi = 5.7$, appropriate for NGC 3379 (Milgrom & Sanders 2003). Had we had the means of obtaining the dynamical surface density distributions of such galaxies we would expect to see an analog of the ring in them (the surface density is a semi-local quantity—density integrated only along the line of sight—in which features appear more distinctly). However, the presently applied methods of mapping the potential field are not good at deducing the local surface densities. This is certainly true of measuring the potential field via velocity dispersion curves of test particles (as in Romanowsky et al. 2003). The most accurate method to date for mapping the potential field of disc galaxies is via rotation curve analysis. Can the transition feature be seen directly on the rotation curve, which measures volume integrated masses? Looking at Fig. 2 we see that the forms of interpolating function that are most conducive to the visibility of a ring in the surface density distribution (e.g. $\bar{\mu}_\alpha$ with $\alpha \geq 2$) could produce features in the rotation curve that are not related to the underlying observable mass distribution—i.e., orphan features—provided the galaxy is an HSB one. Such a feature, which according to MOND can appear only in HSB galaxies, and only at the location of the MOND transition, is to be distinguished from the many known rotation-curve features whose origin can be traced to features in the mass distribution. The latter can appear in all galaxies and anywhere in a galaxy and, unlike the orphan feature, they show up in the Newtonian rotation curve (without DM). A famous case in point is the feature in NGC 1560 (Broeils 1992).

Of course, the transition from a Keplerian to a constant rotational speed is itself a MOND transition feature; but, it is less distinctive than a marked dip, and much less discriminative among the various forms of the interpolating function.

Until recently, almost all disc galaxies with reported rotation curves and MOND analysis had $\xi \leq 1$; for these the form of the interpolating function makes very little difference in the predicted rotation curve; in particular, there is no prediction of an appreciable orphan feature on the rotation curve. This lack of data and analysis has been remedied by Sanders & Noordermeer (2007). They presented MOND analysis of a sample of HSBs, using μ_1 for their MOND fits; this, as we saw, does not produce a distinct feature even under the most favorable conditions [Figs. 2-3, and the discussion below eq.(15)].

On the other hand there were indeed some features on the observed rotation curves that were not reproduced by the MOND curves in the analysis of Sanders and Noordermeer (2007). (These are also not explained by cold dark matter (CDM) fits, such as NFW profiles; see Noordermeer 2006.) We have now analyzed some of these galaxies with choices of μ from our new arsenal. Interestingly, some of these reproduce the previously unexplained orphan features.

Figure 8 shows the observed rotation curves of four spiral galaxies: UGC 128, a low surface brightness (LSB) galaxy with $\xi < 1$ (Sanders 1996); NGC 6503, a “normal” disc galaxy with $\xi \approx 1$ (Begeman et al. 1991); and two HSB galaxies from the sample of Sanders & Noordermeer (2007) with $\xi > 1$. We show the curves predicted by MOND from the observed mass distribution using both μ_1 (reproducing the fits of Noordermeer and Sanders) and $\bar{\mu}_2$. We see that for the first two galaxies (with $\xi \leq 1$) there is very little difference between the two predictions; and there are no orphan features to be found. However, for the two HSB galaxies, there is a clear indication of an orphan feature in the observed curves at the point near the transition from the Newtonian regime to the MOND regime. Moreover, this feature is reproduced by $\bar{\mu}_2$ but not by μ_1 . However, E. Noordermeer (2007, private communication) warns that these galaxies are barred and that the dips in the rotation curves may be due to non-circular motions, and not to true features of the potential field.

While the MOND rotation curves of LSB galaxies are quite insensitive to the form of the interpolating function, those of HSB galaxies are rather sensitive. This raises the possibility that with the new forms of μ studied here we may solve a long standing problem concerning NGC 2841. This is an HSB galaxy that has posed a puzzle in the context of MOND. Begeman Broeils & Sanders (1991), and more recently Bottema & al. (2002), found that a very good MOND fit for the rotation curve of this galaxy is obtained if the galaxy is at a distance somewhat larger than 20Mpc. Putting it at its Hubble distance of 9.46Mpc (as in the former analysis), or even at the more recently determined Cepheid distance of 14.1 ± 1.5 Mpc (as in the latter analysis) gave an inferior fit. Both analyses used μ_2 . We now find that with some of our new interpolating functions, which are also expedient for ring formation, the MOND fit is very good for the Cepheid distance of NGC 2841. We show in Fig. 9 the fit

with μ_2 , reproducing the old conundrum, and we see that using μ_1 alleviates the discrepancy somewhat but not completely. The forms $\bar{\mu}_2$ and $\bar{\mu}_{1.5}$ do a much better job. This may then be the correct solution to the puzzle: not to put NGC 2841 at a larger distance but to use a more appropriate form of μ (a combination of the two is also possible, of course). It should be noted, however, that the larger distance of 23Mpc is indicated both by the Tully-Fisher (TF) relation and by a type Ia supernova in NGC 2841; so the issue remains moot.

To summarize, we may have evidence from rotation curves that the form of the interpolating function conducive to the appearance of a ring of phantom matter, may also be that which is appropriate for the matching of rotation curves in HSB (and LSB) discs. We can also tentatively identify the previously unexplained dips in the observed rotation curves of UGC 3546 and UGC 11670 as the orphan features associated with the MOND transition.

Famaey & Binney (2005) found in their MOND analysis of the Milky Way rotation curve, that it is best fitted with a μ form that starts as $\mu_1(x)$ at small x , then increase faster and become similar to $\mu_2(x)$ at larger x . Our $\bar{\mu}_2$, $\bar{\mu}_3$ also start as μ_1 at small x and then go quickly to 1 (but rather more quickly than in the form used by Famaey and Binney).

The time is becoming ripe for a comprehensive MOND analysis of rotation curves, and other data, to better constrain the form of the interpolating function. The inclusion of the consideration of the orphan, MOND-transition feature adds a new dimension to this sort of analysis.

6. Summary and Discussion

We have shown that, under certain conditions, the PDM distribution in MOND exhibits a maximum along some surface whose scale is largely determined by the MOND transition radius of the underlying (baryonic) mass. This appears without there being a corresponding feature in the underlying source distribution. In axisymmetric configurations aligned with the line of sight this can appear as a ring of DM at that radius, which is unrelated to a length scale characterizing the source. This is expected to hold in any theory of modified dynamics (not only MOND) at the radius that marks the transition from the Newtonian regime to the modified regime. For example, in theories where the transition to modified gravity occurs at a fixed length scale, the feature would appear at that length scale regardless of the mass of the object.

Thus, the statement of Jee et al. (2007) to the effect that the appearance of such an orphan feature is a direct proof of DM, and that it disagrees with modified dynamics interpretation, is incorrect. In fact, the observed parameters of the observed ring in the

galaxy cluster Cl 0024+17 (radius, surface density, contrast, and the mass involved) can be naturally reproduced with this pure MOND phenomenon. The Jee et al. ring may thus turn out to constitute a direct evidence for MOND in action.

For a mass that is well contained within its transition radius, the ring appears quite generically and for a wide range of MOND interpolating functions. The exact properties of the ring depend, however, sensitively on the choice of interpolating function; if enough rings of this type are detected important constraints on that function may emerge. Because the surface density of the ring cannot, generically, much exceed Σ_0 it is easily overwhelmed by the source distribution itself, and so is not expected to appear very commonly in the total mass distribution of realistic configurations (unless we can confidently subtract the underlying source distribution). The properties of the feature also depend strongly on the distribution of the source mass along the line of sight, demonstrating clearly the gross inapplicability of the thin-lens approximation in MOND.

We have not considered non-axisymmetric configurations, but it is expected that in such cases the feature will appear distorted in shape, perhaps broken or irregular.

Furthermore, we found preliminary evidence of a conspicuous orphan feature (a dip) on the rotation curves of some HSB galaxies, that can be identified with the transition from the Newtonian regime to the MOND regime— a feature predicted by MOND with just the forms of the interpolating function that are most conducive in our sample to the appearance of a ring in the PDM surface density distribution. This calls for a reconsideration of the rotation curves of spiral galaxies using these alternative forms of the interpolating function, and possibly others, as well as a systematic study of the implied PDM density distribution in individual galaxies.

Finally, it should be recalled that we have used the algebraic relation, which allowed us to treat and compare many cases, but which for non-spherical systems is only approximate. In a proper treatment of gravitational lensing in the context of a theory inspired by TeVeS, one should solve the non-linear Bekenstein-Milgrom field equation for a given mass distribution.

This research was supported, in part, by a center of excellence grant from the Israel Science Foundation.

REFERENCES

- Aguirre A., Schaye J., & Quataert E., 2001, ApJ, 561, 550

- Angus, G.W., Famaey, B., & Buote, D.A. 2007, MNRAS, submitted; arXiv:0709.0108
- Angus, G.W., Shan, H.Y, Zhao, H.S., & Famaey, B. 2007 ApJ, 654, L13
- Begeman, K. G., Broeils, A. H., & Sanders, R. H. 1991, MNRAS 249, 523
- Bekenstein, J.D. 2004, Phys. Rev. D70, 083509
- Bekenstein, J.D. 2006, Contemporary Physics 47, 387
- Bekenstein, J. & Milgrom, M. 1984, ApJ, 286, 7
- Bissantz, N., Englmaier, P., & Gerhard, O. 2003, MNRAS 340, 949
- Bottema, R., Pestaña, J.L.G., Rothberg, B., & Sanders, R.H. 2002, AA, 393, 453
- Brada, R. & Milgrom, M. 1999, ApJ, 512, L17
- Broeils, A. H. 1992, AA, 256, 19
- Bruneton, J.P. & Esposito-Farese, G. 2007, Phys. Rev. D, 76, 124012
- Clowe, D., Bradac, M. Gonzalez, A.H., Marevitch, M., Randall, S.W., Jones, C., & Zaritsky, D., 2006, ApJ, 648, L109
- Famaey, B., Angus, G.W., Gentile, G., Shan, H.Y., & Zhao, H.S. 2007a, AA, submitted, arXiv:0706.1279
- Famaey, B., Gentile, G., Bruneton, J.P., & Zhao, H.S. 2007b, Phys. Rev. D 75, 063002
- Famaey, B. & Binney, J. 2005, MNRAS, 363, 603
- Gerbal, D., Durret, F., Lachieze-Rey, M., & Lima-Neto, G. 1992, AA, 262, 395
- Jee, M.J., Ford, H.C., Illingworth, G.D., White, R.L., Broadhurst, T.J., Coe, D.A., Meurer, G.R., Van Der Wel, A., Benitez, N., Blakeslee, J.P. Bouwens, R.J., Bradley, L.D., Demarco, R., Homeier, N.L., Martel, A.R., & Mei, S. 2007, ApJ, 661, 728
- Kent, S.M. 1987, AJ, 93, 816
- Milgrom, M. 1983a, ApJ, 270, 365
- Milgrom, M. 1983b, ApJ, 270, 371
- Milgrom, M. 1986a, ApJ, 302, 617

- Milgrom, M. 1986b, ApJ, 306, 9
- Milgrom, M. 1994, Ann. Phys. 229, 384
- Milgrom, M. 2001, MNRAS, 326, 1261
- Milgrom, M. 2002, New Astronomy Review, 46, 741
- Milgrom, M. 2008, arXiv:0801.3133; to be published in the Proceedings of the XIX Rencontres de Blois.
- Milgrom, M. & Sanders, R.H. 2003, ApJ, 599, L25
- Milgrom, M. & Sanders, R.H. 2005, MNRAS, 357, 45
- Mortlock, D.J. & Turner, E.L. 2001, MNRAS, 327, 557
- Noordermeer 2006, PhD Thesis, University of Groningen
- Pointecouteau, E. & Silk, J. 2005, MNRAS, 364, 654
- Romanowsky, A.J., Douglas, N.G., Arnaboldi, M., Kuijken, K., Merrifield, M.R. Napolitano, N.R., Capaccioli, M., & Freeman, K.C. 2003, Science, 301, 1696
- Sanders, R.H. 1996, ApJ, 473, 117
- Sanders, R.H. 1999, ApJ, 512, L23
- Sanders, R.H. 2003, MNRAS, 342, 901
- Sanders, R.H. 2007, MNRAS, 380, 331
- Sanders, R.H. & McGaugh, S.S. 2002, ARA&A, 40, 263
- Sanders, R.H. & Noordermeer, E. 2007, MNRAS, 379, 702
- Zhang, Y.-Y., Böhringer, H., Mellier, Y., Soucail, G., & Forman, W. 2005, AA, 429, 85
- Zhao, H. S. & Famaey, B. 2006, ApJ, 638, L9
- Zlosnik, T.G., Ferreira, P.G., & Starkman, G.D. 2007, Phys. Rev. D 75, 044017

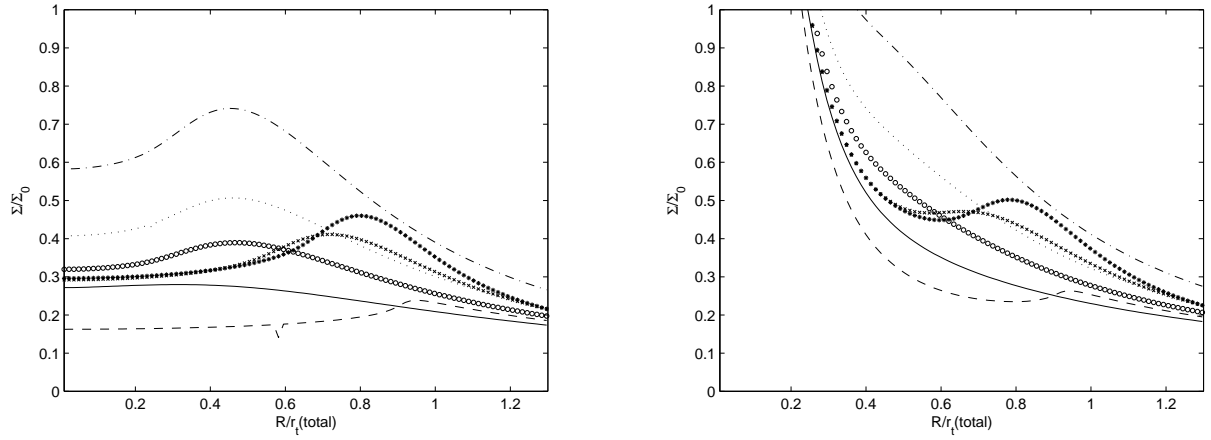


Fig. 7.— The projected Surface density, in units of Σ_0 , for a de Vaucouleurs model with $R_e = r_t/5.7$, appropriate for NGC 3379. On the left is shown the PDM alone, and on the right the total. The interpolating functions used are: μ_2 (solid), μ_{50} (dashed), $\tilde{\mu}_1$ (dotted), $\tilde{\mu}_2$ (dashed-dotted), $\bar{\mu}_1$ (circles), $\bar{\mu}_2$ (crosses), $\bar{\mu}_3$ (stars).

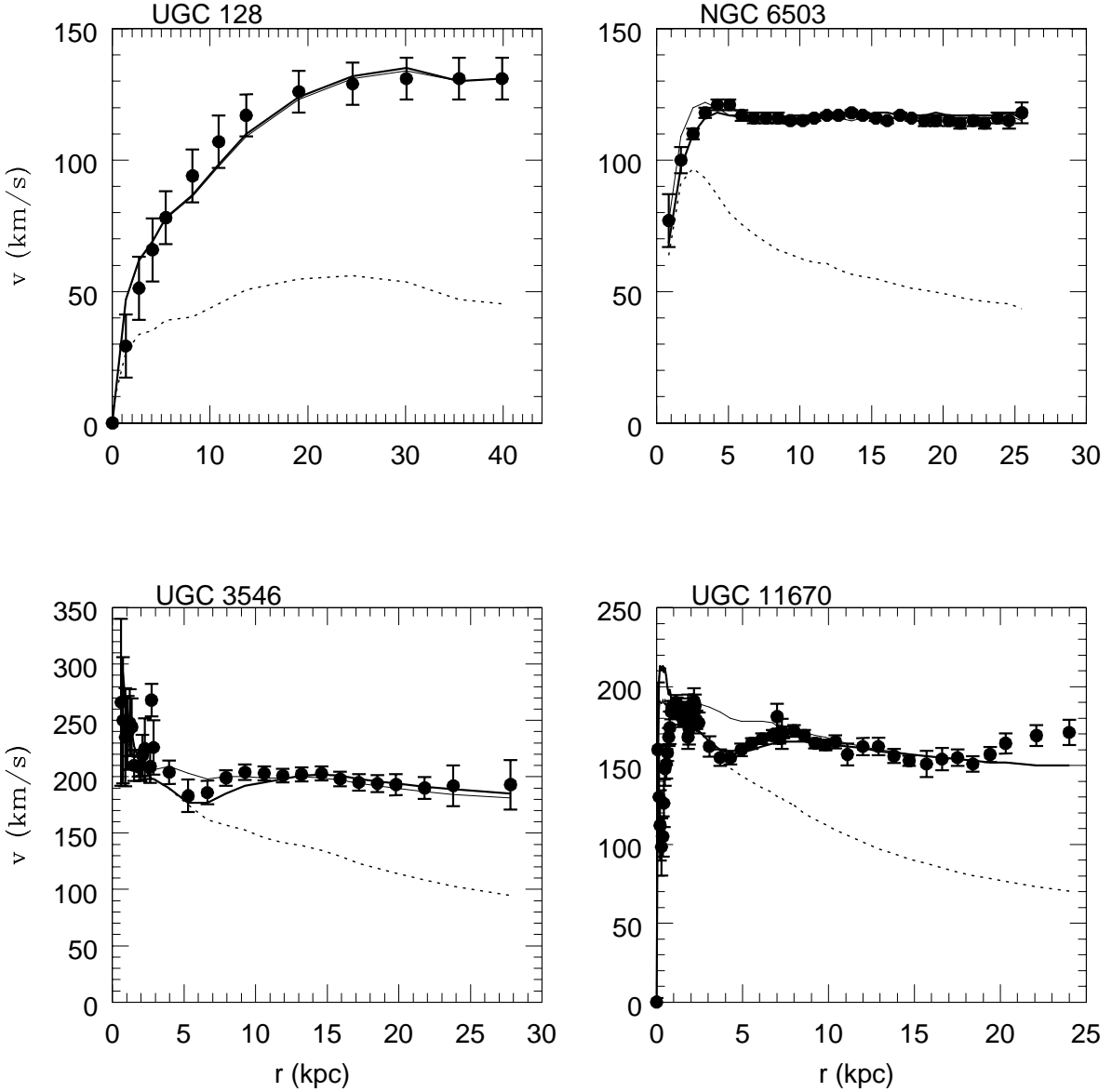


Fig. 8.— MOND rotation curves for four galaxies. UGC 128 is a low surface brightness galaxy (Sanders 1996); NGC 6503 is a typical spiral galaxy with average surface brightness (Begeman et al. 1991); UGC 3546 and UGC 11670 are two high surface brightness galaxies from the sample of Noordermeer (Sanders & Noordermeer 2007). The points with error bars are the observations. Also shown are the calculated rotation curves: MOND for $\bar{\mu}_2$ (solid thick), and MOND for μ_1 (solid thin). The best fit M/L values in solar units are: 1.0 for UGC 128 (disc only, both fits); 0.9 for NGC 6503 (disc only, both fits). UGC 3546: 2.5 (disc) and 7.0 (bulge) for $\bar{\mu}_2$, 2.5 (disc) and 5.9 (bulge) for μ_1 . UGC 11670: 2.5 (disc) and 4.5 (bulge) for $\bar{\mu}_2$, 3.0 (disc) and 3.5 (bulge) for μ_1 . Newtonian curves (dotted) are given for the M/L values from the $\bar{\mu}_2$ fits.

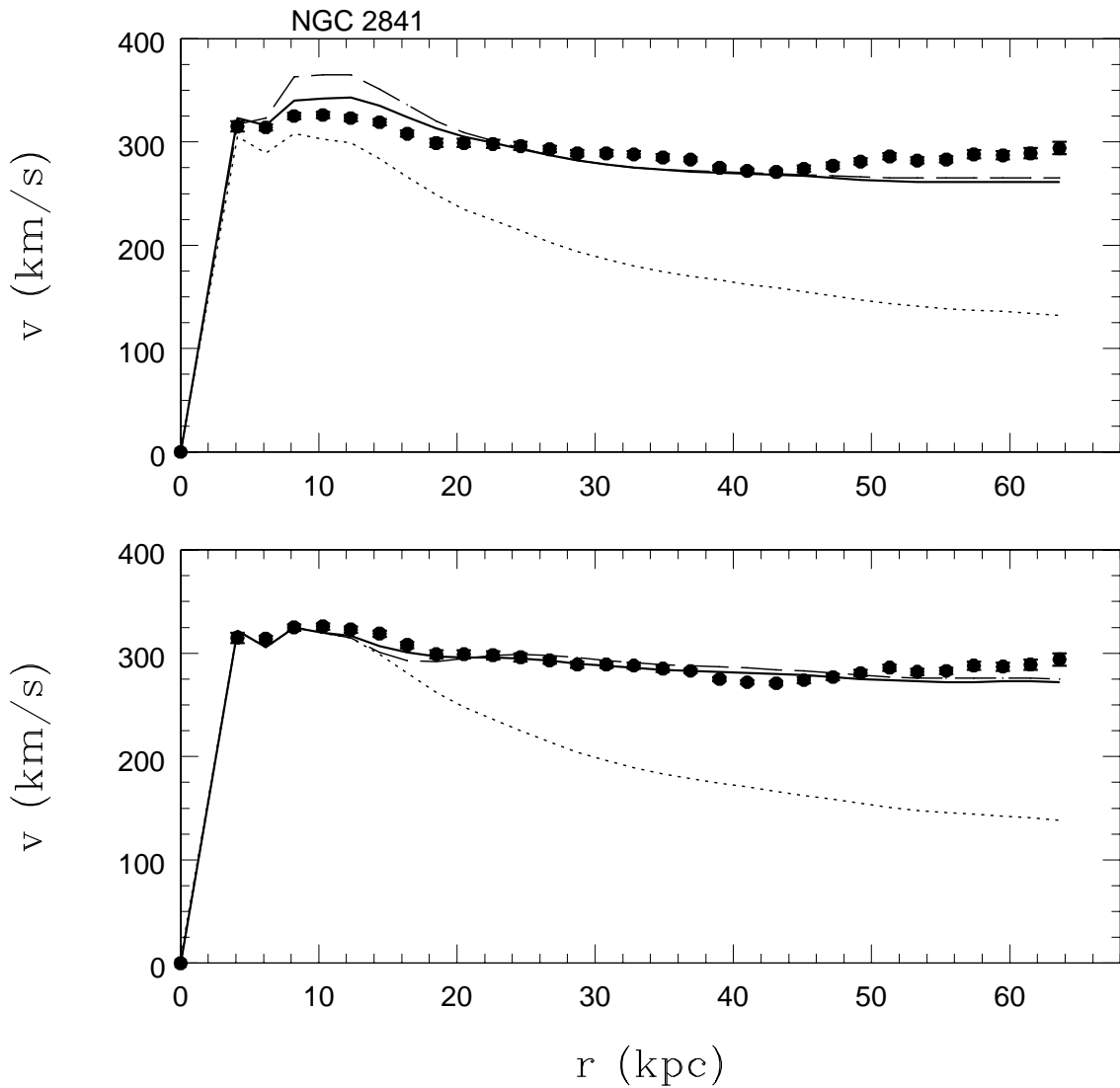


Fig. 9.— The MOND rotation curves of NGC 2841 for different choices of the interpolating function compared with the data (points). The best fit M/L values in solar units are given below in parentheses for the disc and bulge respectively. Upper panel: μ_2 in dashed line (8.1, 1.0); μ_1 in solid line (4.9, 2.5); Newtonian curve with M/L values for μ_1 (dotted). Lower panel: $\bar{\mu}_2$ in dashed line (5.4, 2.8); $\bar{\mu}_{1.5}$ in solid line (5.4, 2.8); Newtonian curve (dotted).